Pediatric Cerebral Stroke: Susceptibility-Weighted Imaging May Predict Post-Ischemic Malignant Edema

THANGAMADHAN BOSEMANI, ANDREA PORETTI, GUNES ORMAN, AVNER MEODED, THIERRY A.G.M. HUISMAN

Section of Pediatric Neuroradiology, Division of Pediatric Radiology, Russell H. Morgan Department of Radiology and Radiological Science, The Johns Hopkins University School of Medicine; Baltimore, MD, USA

Key words: susceptibility-weighted imaging, children, neuroimaging, stroke, hyperperfusion, post-ischemic malignant edema

SUMMARY – *Susceptibility-weighted imaging (SWI) is an advanced MRI technique providing information on the blood oxygenation level. Deoxyhemoglobin is increased in hypoperfused tissue characterized by SWI-hypointensity, while high oxyhemoglobin concentration within hyperperfused tissue results in a SWI iso- or hyperintensity compared to healthy brain tissue. We describe a child with a stroke, where SWI in addition to excluding hemorrhage and delineating the thrombus proved invaluable in determining regions of hyperperfusion or luxury perfusion, which contributed further to the prognosis including an increased risk of developing post-ischemic malignant edema.*

Introduction

Neuroimaging plays a key role in the diagnosis of acute ischemic stroke (AIS) in children [1]. Conventional and advanced MR sequences such as diffusion-weighted imaging (DWI) and perfusion-weighted imaging (PWI) can confirm pediatric AIS and rule out mimickers. Moreover, a combined analysis of DWI and PWI data may identify tissue at risk of progressing infarction, and guide treatment.

Susceptibility-weighted imaging (SWI) was recently shown to be a useful complementary MR sequence in the evaluation of pediatric AIS [2-7]. SWI may detect hemorrhages within the infarcted tissue and evaluate the ischemic penumbra focusing on the signal intensity within the draining veins [3-7].

We report on SWI and arterial spin labeling (ASL) findings in pediatric AIS and show how SWI may add information in the detection of early reperfusion/hyperperfusion.

Case Report

A six-year-old girl with Down syndrome presented with acute left hemiplegia and central facial nerve palsy as well as left-sided neglect and gaze preference. The clinical findings were suspicious of an acute ischemic stroke involving the right middle cerebral artery (MCA) territory. Head CT imaging obtained at an outside institution about one hour after onset of symptoms showed a hyperdense thrombus in the right MCA and a faint hypodensity of the involved white matter compatible with acute thrombotic right MCA ischemic stroke, and led to admission to our tertiary pediatric center for further management.

Brain MRI was obtained on a 3.0 T scanner (Skyra, Siemens, Erlangen, Germany) about eight hours after onset of symptoms. Standard departmental protocol including T1, T2 and FLAIR imaging was applied. In addition, we acquired: 1) a single-shot spin-echo echo-planar

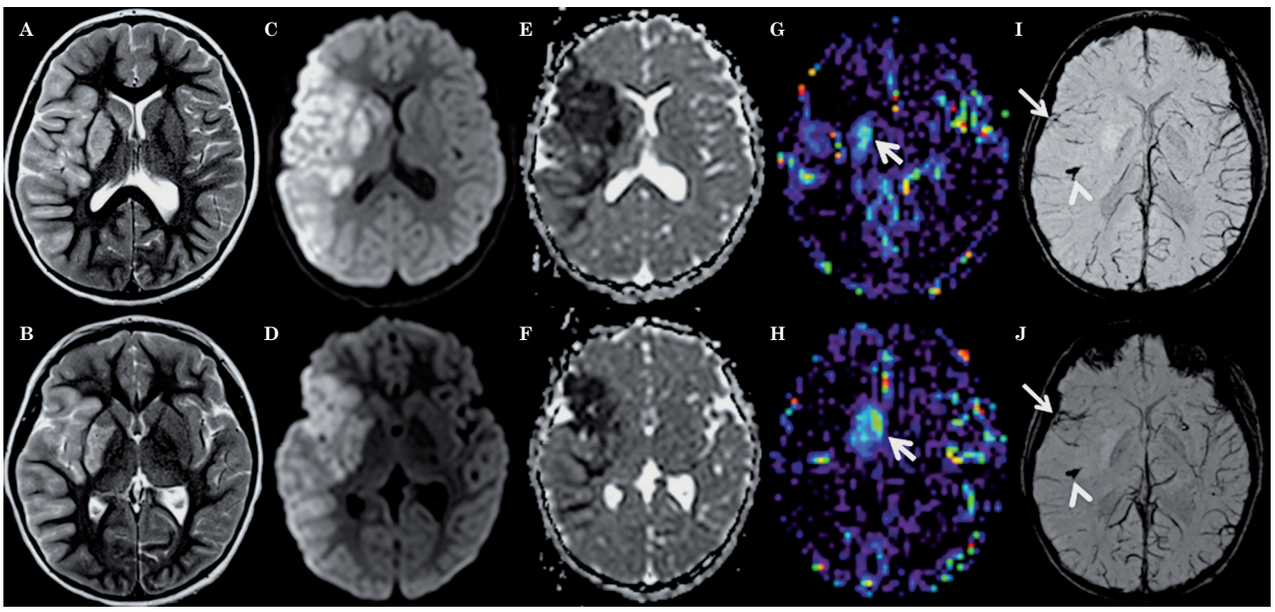

Figure 1 Axial T2-weighted (A,B), trace of diffusion (C,D), ADC maps (E,F), CBF-ASL maps (G,H) and minIP-SWI images (I,J) 8 hours after onset of symptoms show T2 hyperintense signal abnormalities and restricted diffusion (hyperintense signal abnormality on C,D with matching low ADC values on E,F) involving the cortex as well as subcortical and deep white matter within the right MCA territory as well as right putamen and caudate nucleus. Restricted diffusion in the anterior tip of the right temporal lobe and insula matches the territory drained by SWI hypointense sulcal veins (arrows on I,J). The rest of the right MCA territory appears less affected on ADC maps and the sulcal veins draining this territory appear less prominent and especially less SWI hypointense suggesting lower oxygen extraction fraction. In these parts of the right MCA territory, CBF-ASL maps appear symmetrical to the contralateral MCA territory suggesting relative normal perfusion. The veins draining the right anterior basal ganglia are less SWI hypointense matching increased absolute CBF on the ASL map demonstrating hyperperfusion (arrows on G,H). Additionally, the minIP SWI images demonstrate thrombus in the M2 segment of the right MCA with susceptibility artifacts along the course of the vessel (arrowheads in I,J).

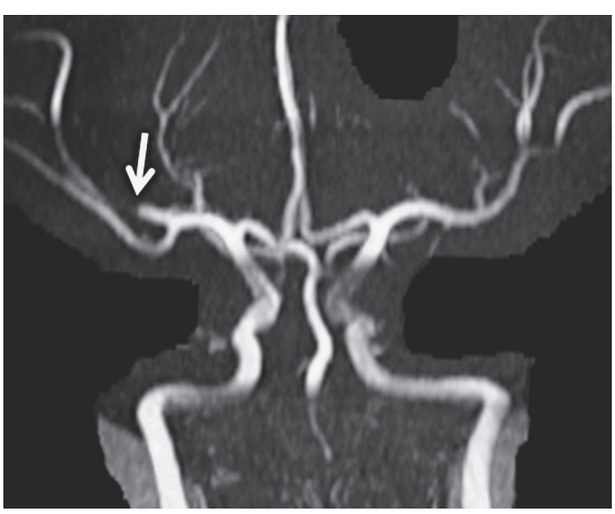

Figure 2 3D-TOF MRA reveals abrupt termination of the distal M1 segment (arrow) with faint reconstitution of small caliber M2 branch of the right MCA.

axial diffusion tensor imaging (DTI) sequence, parameters: 20 orthogonal diffusion directions, *b*-value of 1000 s/mm^2 for each of the 20 diffusion-encoding directions with an additional measurement without diffusion weighting (B-value of 0 s/mm^2), TR 7500 ms, TE 82 ms, slice thickness 2.5 mm, FOV 240×240 mm, matrix size 192×192; trace of diffusion and apparent diffusion coefficient (ADC) maps were calculated from the raw data sets; 2) magnitude and phase axial SWI images, parameters: TR 49 ms, TE 40 ms, flip angle 15°, bandwidth 80 kHz, slice

thickness 2.0 mm, FOV 201×230, matrix size 320×221 iPAT factor of 2; axial 8-mm minimal intensity projection (minIP)-SWI images were reconstructed; 3) axial pulsed ASL with generation of cerebral blood flow (CBF) maps; 4) time-of-flight (TOF) magnetic resonance angiography (MRA) through the circle of Willis and neck with post-processed volumetric 3D reconstruction.

Diffusion restriction was noted on the ADC maps in the right MCA territory, with cortical-subcortical involvement of the right frontal, parietal and temporal lobes, and right basal ganglia (Figure 1C-F). The regions with diffusion restriction demonstrated matching cortical-subcortical T2-hyperintense signal (Figure 1A,B) and mildly increased intravascular, but not parenchymal contrast enhancement on postcontrast T1-weighted images (not shown). These findings were consistent with acute ischemic infarction. There was no evidence of hemorrhagic conversion. 3D-TOF-MRA revealed abrupt termination of the distal M1 segment with faint reconstitution of a small caliber M2 branch of the right MCA (Figure 2). The minIP-SWI images demonstrated a markedly SWI hypointense thrombus in the M2 segment of the right MCA with susceptibility artifacts along the course of the vessel (Figure 1I,J). Additionally, the sulcal veins draining the ischemic right MCA territory appeared less prominent and especially less SWI-hypointense compared to the veins draining non-ischemic brain tissue (Figure 1I,J). The discrepancy of the SWI signal within the draining veins was especially prominent compared to the sulcal veins draining the non-ischemic left MCA territory which showed a normal physiological SWI hypointensity. Detailed analysis of the SWI images also showed that the veins draining the right anterior basal ganglia as well as the right internal cerebral vein were also less SWI hypointense (Figure 1I,J). Moreover, the anterior tip of the right temporal lobe and insula showed focally more normal appearing SWI hypointense draining veins. Finally, the entire right putamen showed a significant parenchymal SWI hyperintensity (Figure 1I,J). The absolute CBF-ASL map demonstrated a hyperperfusion to the right putamen matching the putaminal SWI hyperintensity (Figure 1G,H). The remainder of the right MCA territory with diffusion restriction appeared symmetrical to the contralateral MCA territory suggesting relative normal CBF.

Follow-up head CT 28 hours after onset of symptoms revealed increased hypodense delineation of the infarcted tissue affecting the right basal ganglia, anterior tip of the right temporal lobe and insula (Figure 3A). On continued CT follow-up, progressive cerebral edema developed with midline shift, uncal herniation and secondary right posterior cerebral artery (PCA) territory ischemia requiring emergent decompression with hemicraniectomy six days after onset of symptoms (Figure 3B).

Discussion

SWI is a high-spatial-resolution 3D gradient echo MRI technique accentuating the magnetic properties of blood, blood products, non-heme iron and calcifications [8,9]. Based on these properties, SWI is increasingly used in pediatric and neonatal neuroimaging for the evaluation of hemorrhage, vascular malformations, traumatic brain injury, brain tumors, congenital infections and neurodegenerative disorders [10,11].

SWI has also been shown to be a useful non-contrast enhanced imaging sequence in the evaluation of pediatric AIS [2-7]. SWI may 1) detect hemorrhagic components within the infarcted tissue [12], 2) demonstrate hypointense signals in the veins draining hypoperfused areas and evaluate the ischemic penumbra focusing on venous drainage [3-7], 3) detect acute occlusive arterial thrombo-emboli [9,10], 4) quantify microhemorrhages and predict hemorrhagic transformation before thrombolytic therapy is initiated [13] and 5) detect early hemorrhagic complications after intraarterial thrombolysis [9].

In our patient, SWI gave multiple valuable components of information: 1) SWI excluded secondary hemorrhages within the infarcted tissue; 2) the thrombus in the right MCA was easily identified by its prominent SWI hypointensity (similar to the well-known hyperdense thrombus sign on CT); 3) the asymmetry of the superficial (sulcal veins) and deep draining veins as revealed by SWI matched the area of restricted diffusion; 4) the higher than usual SWI signal intensity of the draining veins suggests luxury perfusion or early reperfusion of ischemic tissue; and 5) the increased parenchymal signal of the putamen on SWI indicates an increased pO2 within the tissue likely secondary to reperfusion/hyperperfusion. On the basis of SWI blood oxygenation level-dependent contrast characteristics, the concentration of oxygenated hemoglobin is increased within the veins draining the right MCA territory and in particular the concentration of oxygenated hemoglobin within the

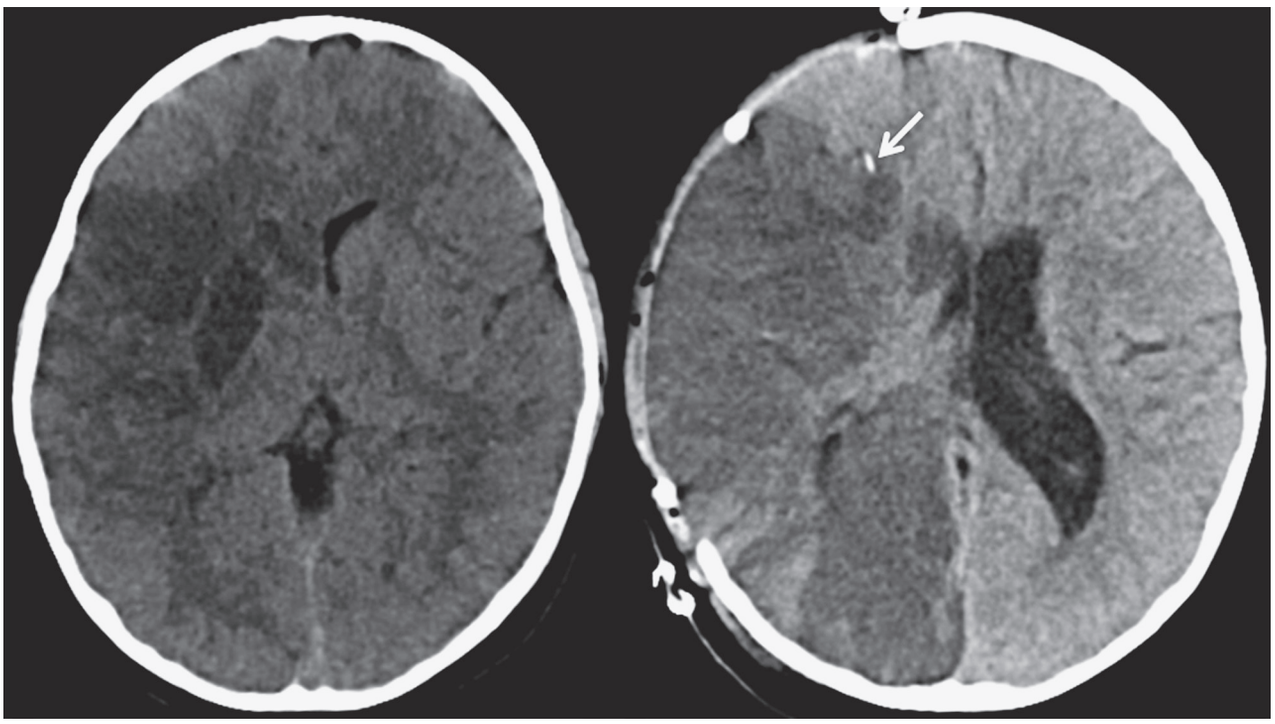

A **B**

Figure 3 A) Follow-up axial CT 28 hours after onset of symptoms revealed a better delineation of the infarcted tissue as hypodensity in the right basal ganglia, anterior tip of the right temporal lobe and insula. B) Follow-up axial CT after hemicraniectomy showed evolving right MCA stroke with secondary involvement of the right PCA, moderate edema of the infarcted regions and mild right to left midline shift. The intracranial pressure monitoring device is noted as a hyperdense focus anterior to the body of the lateral ventricle within the right frontal lobe white matter (arrow).

putamen is increased. These findings are most likely secondary to a luxury perfusion. The matching relative normal perfusion to most of the right MCA territory and the focal hyperperfusion of the right putamen on the CBF-ASL map (Figure 1) confirm the SWI findings.

Early reperfusion/hyperperfusion was shown to result from an overabundant CBF relative to the metabolic needs of the brain tissue that occurs after a period of vascular arrest [14]. Early reperfusion/hyperperfusion may have significant prognostic benefits and may be associated with an improved outcome and smaller infarct size [15]. On the other hand, early reperfusion/hyperperfusion is also linked to an increased risk of developing malignant edema with secondary ischemia requiring decompressive hemicraniectomy [16]. The breakdown of the blood-brain barrier during cerebral reperfusion may lead to the development of vasogenic edema, hypertension and infarction, all contributing to cerebral reperfusion injury [17]. Imaging findings suggesting early reperfusion/hyperperfusion in pediatric AIS should initiate continuous monitoring of intracranial pressure and neurological signs to avoid further brain injury.

In summary, this case highlights the importance of utilizing multiple advanced MRI techniques, in particular the evolving role of SWI in combination with ASL and DWI/DTI to better understand and predict the complex cerebral hemodynamics in pediatric AIS. SWI and PWI may demonstrate hyperperfusion or reperfusion, which should alert clinicians to possible reperfusion injury and malignant/complicating cerebral edema.

Prospective large-scale studies should confirm the significance of SWI hyperintensity for predicting malignant post-ischemic cerebral edema.

References

1 Jones BP, Ganesan V, Saunders DE, et al. Imaging in childhood arterial ischaemic stroke. Neuroradiology. 2010; 52 (6): 577-589.
2 Santhosh K, Kesavadas C, Thomas B, et al. Susceptibility weighted imaging: a new tool in magnetic resonance imaging of stroke. Clin Radiol. 2009; 64 (1): 74-83.
3 Chalian M, Tekes A, Meoded A, et al. Susceptibility-weighted imaging (SWI): a potential non-invasive imaging tool for characterizing ischemic brain injury? J Neuroradiol. 2011; 38 (3): 187-190.
4 Kesavadas C, Thomas B, Pendharakar H, et al. Susceptibility weighted imaging: does it give information similar to perfusion weighted imaging in acute stroke? J Neurol. 2011; 258 (5): 932-934.
5 Meoded A, Poretti A, Benson JE, et al. Evaluation of the ischemic penumbra focusing on venous drainage: the role of susceptibility weighted imaging (SWI) in pediatric ischemic cerebral stroke. J Neuroradiol. 2013. Epub Jul 1.
6 Meoded A, Poretti A, Tekes A, et al. Role of susceptibility-weighted imaging in predicting stroke evolution. Neurographics. 2013; in press.
7 Kao HW, Tsai FY, Hasso AN. Predicting stroke evolution: comparison of susceptibility-weighted MR imaging with MR perfusion. Eur Radiol. 2012; 22 (7): 1397-1403.
8 Haacke EM, Mittal S, Wu Z, et al. Susceptibility-weighted imaging: technical aspects and clinical applications, part 1. Am J Neuroradiol. 2009; 30 (1): 19-30.
9 Mittal S, Wu Z, Neelavalli J, et al. Susceptibility-weighted imaging: technical aspects and clinical applications, part 2. Am J Neuroradiol. 2009; 30 (2): 232-252.
10 Verschuuren S, Poretti A, Buerki S, et al. Susceptibility weighted imaging of the pediatric brain. AJR Am J Roentgenol. 2012; 198 (5): W440-W449.
11 Meoded A, Poretti A, Northington FJ, et al. Susceptibility weighted imaging of the neonatal brain. Clin Radiol. 2012; 67 (8): 793-801.
12 Wycliffe ND, Choe J, Holshouser B, et al. Reliability in detection of hemorrhage in acute stroke by a new three-dimensional gradient recalled echo susceptibility-weighted imaging: technique compared to computed tomography: a retrospective study. J Magn Reson Imaging. 2004; 20 (3): 372-377.
13 Akter M, Hirai T, Hiai Y, et al. Detection of hemorrhagic hypointense foci in the brain on susceptibility-weighted imaging clinical and phantom studies. Acad Radiol. 2007; 14 (9): 1011-1019.
14 Lassen NA. The luxury-perfusion syndrome and its possible relation to acute metabolic acidosis localised within the brain. Lancet. 1966; 2 (7473): 1113-1115.
15 Chen J, Licht DJ, Smith SE, et al. Arterial spin labeling perfusion MRI in pediatric arterial ischemic stroke: initial experiences. J Magn Reson Imaging. 2009; 29 (2): 282-290.
16 Marchal G, Young AR, Baron JC. Early postischemic hyperperfusion: pathophysiologic insights from positron emission tomography. J Cereb Blood Flow Metab. 1999; 19 (5): 467-482.
17 Pan J, Konstas AA, Bateman B, et al. Reperfusion injury following cerebral ischemia: pathophysiology, MR imaging, and potential therapies. Neuroradiology. 2007; 49 (2): 93-102.

Thierry A.G.M. Huisman, MD
Division of Pediatric Radiology
The Russell H. Morgan Department of Radiology and Radiological Science
The Johns Hopkins School of Medicine
Charlotte R. Bloomberg Children's Center
Sheikh Zayed Tower, Room 4174, 1800 Orleans Street
Baltimore, MD 21287-0842, USA
Tel.: +14109556454
Fax: +14105023633
E-mail: thuisma1@jhmi.edu